An update of the LDEO fCO_2-Residual method: algorithmic choices improve ocean carbon sink estimates

Thea H. Heimdal[1], Amanda R. Fay[1], Abby P. Shaum[1], Viviana Acquaviva[2,1], Val Bennington[3], Amelie E. Sharples[1], Nicoline M. Joenson[1] & Galen A. McKinley[1]

[1]Columbia University and Lamont-Doherty Earth Observatory, Palisades, NY, USA
[2]New York City College of Technology, City University of New York, Brooklyn, NY, USA
[3]Makai Ocean Engineering, Waimanalo, HI, USA

Correspondence to: Thea H. Heimdal (theimdal@ldeo.columbia.edu)

This manuscript is a non-peer reviewed preprint submitted to EarthArXiv. This manuscript has been submitted for publication in Machine Learning:Earth, and is currently undergoing peer-review.

Abstract

We evaluate the impact of various algorithmic design choices on reconstruction skill and estimated air-sea CO_2 flux using the fCO_2-Residual machine learning (ML) method (Bennington et al., 2022a) to reconstruct surface ocean fCO_2. We reconstruct fCO_2 globally over the period 1982-2023 by optimizing the hyperparameter selection process ($Residual^{OPT}$) and/or using ΔfCO_2-Residual (subtracting fCO_2^{atm} from fCO_2^{ocn}) as a target variable ($\Delta Residual^{OPT}$). We compare these reconstructions to the original fCO_2-Residual approach ($Residual^{ORG}$) from Bennington et al. (2022a). We find general agreement between the three approaches for the majority of the analysis period, but there are significant differences towards the beginning and end. Compared to $Residual^{ORG}$, $\Delta Residual^{OPT}$ and $Residual^{OPT}$ show stronger ocean carbon uptake in the 1980s, with a global mean difference over 1982-1987 of 0.6 and 0.4 PgC/yr, respectively. In 2023, the global mean air-sea CO_2 flux for both approaches is reduced by 0.4 PgC/yr. The test error metrics show that the highest reconstruction skill is achieved for $\Delta Residual^{OPT}$. We present an additional analysis of reconstruction fidelity of the fCO_2-Residual method by using a testbed of CMIP6 Earth System Models to reconstruct fCO_2. The testbed analysis is in agreement with the observation-based test error metrics; both approaches improve reconstruction skill compared to $Residual^{ORG}$, but $\Delta Residual^{OPT}$ leads to the lowest reconstruction errors for the full analysis period (1982-2023). We

conclude that, for the fCO_2-Residual method, the impacts of algorithmic design choices (i.e., hyperparameters or target variable) on reconstruction skill and estimated air-sea CO_2 fluxes are significant, and it is possible to improve reconstruction fidelity even without the availability of additional observations.

Keywords: ocean carbon, ocean sink, air-sea CO_2 flux

1. Introduction

Quantifying the ocean carbon sink across time and space is crucial in order to understand current and future changes to Earth's climate. The Global Carbon Budget (GCB) presents annual estimates of the global ocean carbon uptake based on ensembles of 10 global ocean biogeochemistry models (GOBMs) and eight observation-based data products (hereafter referred to as "data products") (Friedlingstein et al., 2025). These 18 ocean carbon sink estimates show a large spread, and the best estimate presented in the GCB has a large uncertainty (0.4 PgC/yr; Friedlingstein et al., 2025). There are numerous sources that may contribute to uncertainties in ocean carbon sink estimates. Here, we focus on uncertainties related to data products' reconstruction skill; i.e., their ability to reconstruct surface ocean fCO_2 (fugacity of CO_2).

All GCB data products utilize the same database of monthly 1°x1° gridded surface ocean fCO_2 measurements from the Surface Ocean CO_2 ATlas (SOCAT; Bakker et al., 2016). SOCAT is the largest quality-controlled database of in situ fCO_2 observations in sea surface waters for the global ocean and coastal zones, containing more than 30 million high-quality (uncertainty of < 5 µatm) measurements. The data products reconstruct surface ocean fCO_2 across space and time where SOCAT observations do not exist, by using statistical methods and machine learning (ML) techniques (e.g., Landschützer et al., 2016; Iida et al., 2021; Rödenbeck et al., 2022; Gloege et al., 2022; Bennington et al., 2022a,b; Ford et al., 2024). The SOCAT database only covers roughly 2% of the surface ocean at monthly 1°x1° spatial resolution over the period of 1982-2024; this data sparsity contributes to the reconstruction errors shown by the data products (e.g., Gloege et al., 2021; Hauck et al., 2023).

Improvements in reconstructing surface ocean fCO_2 can be achieved by consistently adding more observations, especially in the Southern Ocean (e.g., Gloege et al., 2021; Hauck et al., 2023; Behncke et al., 2024; Dong et al., 2024; Heimdal et al., 2024, Fay et al., 2025). However, this

requires significant increase in funding for ocean observing, deployment of high-quality autonomous platforms at scale (e.g., Sutton et al., 2021), bias corrections of float-derived fCO_2 estimates (Williams et al., 2017; Heimdal & McKinley, 2024), or new technology. Recent studies have explored other ways to improve the estimates produced by data products, such as pre-processing data (Bennington et al., 2022a,b; Gloege et al., 2022; Gregor et al., 2024), increasing spatial resolution (Gregor et al., 2024), algorithm optimization (Zhong et al. 2024; Heimdal et al., 2025) or changing the algorithm target variable from fCO_2 to ΔfCO_2 ($\Delta fCO_2 = fCO_2^{ocean} - fCO_2^{atm}$) (Gregor et al., 2024; Wanninkhof et al., 2025).

Here, we assess changes in reconstructed fCO_2 and estimated air-sea CO_2 flux due to algorithm optimization and the choice of algorithm target variable for one data product, the Lamont-Doherty Earth Observatory (LDEO) fCO_2-Residual method (Bennington et al., 2022a). Note that the fCO_2-Residual method already includes a pre-processing step that has been shown to reduce reconstruction error: the direct effect of temperature on fCO_2 is removed prior to algorithm processing ($fCO_2 - fCO_2\text{-T} = fCO_2\text{-Residual}$; Bennington et al., 2022a). The target variable of the fCO_2-Residual method is therefore "fCO_2-Residual", which means that the algorithm only has to learn the biogeochemical/physical component of fCO_2. Additionally, a previous study showed, by using a testbed of CMIP6 Earth System Models, that significant reductions in reconstruction error for the fCO_2-Residual method is possible without adding new observations (Heimdal et al., 2025). Instead, reconstruction fidelity was improved by selecting algorithm hyperparameters on the basis of reducing reconstruction bias. Here, we implement this algorithmic design choice for the observation-based fCO_2-Residual method, by targeting bias in the algorithm optimization process ($Residual^{OPT}$). We assess the change in air-sea CO_2 flux and reconstruction skill compared to the original fCO_2-Residual method from Bennington et al. (2022a) ($Residual^{ORG}$).

Further, it has been shown that the long-term increase in fCO_2 may negatively impact the ability of algorithms to represent the data, which may lead to reconstruction biases, and ultimately an over- or underestimation of the ocean carbon sink (Gloege et al., 2022; Hauck et al., 2023; Gregor et al., 2024; Wanninkhof et al., 2025; Heimdal et al., 2025). Algorithms perform best when the target and predictor variable distributions have the same shape (Goodfellow et al., 2016; Gloege et al., 2022). Many of the predictor variables used in fCO_2 reconstructions (e.g., salinity, chlorophyll) do not show significant temporal trends that are evident in oceanic fCO_2 values. Thus,

the data products that reconstruct fCO_2 must predict a right-skewed data distribution that does not match those of the predictor variables (Gloege et al., 2022). Two recent studies showed reduced reconstruction error when removing the long-term trend of fCO_2 from the algorithm target variable (Gregor et al., 2024; Wanninkhof et al., 2025). Here, we implement this approach for the fCO_2-Residual method, by switching from fCO_2-Residual to ΔResidual as the target.

Finally, to further assess the fidelity of reconstruction error between the three approaches, we employ the testbed approach from Heimdal et al. (2025). Instead of using actual SOCAT observations to reconstruct surface ocean fCO_2, the algorithmic training set is sub-sampled from a testbed of CMIP6 models. A testbed provides a correct solution (the testbed truth) against which the reconstructed fCO_2 can be directly evaluated. This allows for comparisons that reveal the influence and error in reconstructed fCO_2 between the three approaches: $\text{Residual}^{\text{OPT}}$, $\text{Residual}^{\text{ORG}}$ and $\Delta\text{Residual}^{\text{OPT}}$.

The goal of this work is to assess whether it is possible to improve reconstruction skill of the original fCO_2-Residual method (Bennington et al., 2022a) without specifically adding additional observations, but through algorithmic design choices such as algorithm optimization and the choice of target variable. This work improves our understanding of how algorithmic choices impact reconstruction skill and the estimated air-sea CO_2 flux, and allows better understanding of the validity of current estimates of the ocean carbon sink.

2. Methods

2.1 The fCO_2-Residual method

We use the fCO_2-Residual method (Bennington et al., 2022a) to reconstruct fCO_2 globally over 1982-2023 using monthly 1°x1° gridded observations from SOCATv2024 (Bakker et al., 2024; **Section 2.2**) and the CMIP6-testbed (**Section 2.3**). A brief description of the fCO_2-Residual method is provided below; for further details see Bennington et al. (2022a). The first step of the fCO_2-Residual method is to remove the direct effect of temperature on fCO_2. This temperature-driven component (fCO_2-T) is calculated using the equation of Takahashi et al. (2002):

$$\textbf{\textit{Equation 1:}}\ fCO_2T = \underline{fCO_2} \times exp.[0.0423 \times (SST - \underline{SST})]$$

where the overbars represent the long-term global means of fCO_2 and sea surface temperature (SST), respectively. The fCO_2-Residual is calculated by subtracting fCO_2-T from fCO_2:

Equation 2: $fCO_2\text{-Residual} = fCO_2 - fCO_2\text{-T}$

To calculate ΔfCO_2-Residual, the global mean atmospheric CO_2 (xCO_2 ppm × pressure) is then subtracted from fCO_2-Residual:

Equation 3: $\Delta fCO_2\text{-Residual} = fCO_2\text{-Residual} - CO_2^{atm}$

The eXtreme Gradient Boosting algorithm method (XGB; Chen & Guestrin, 2016) is used to develop a Machine Learning (ML) model that predicts the target variable from the predictor variables which act as proxies for processes influencing fCO_2. The target variable is either ΔfCO_2-Residual or fCO_2-Residual. Predictor variables include sea surface temperature (SST), sea surface salinity (SSS), chlorophyll concentration (Chl-a), mixed layer depth (MLD), atmospheric concentration of CO_2 (xCO_2), time of year (T0, T1), geographic location (A, B, C), and interannual anomalies for SST, SSS and Chl-a. The interannual anomalies are calculated by subtracting the monthly climatology (e.g., average of all Januarys, all Februarys, etc.) from the corresponding month. Geographic coordinates and dates are replaced with continuous values between -1 and 1 using N-vector and time transformations to account for periodic boundary conditions (Bennington et al., 2022a). Predictor variables are the same for all reconstructions discussed ($Residual^{OPT}$, $Residual^{ORG}$ and $\Delta Residual^{OPT}$).

To obtain the final reconstruction of fCO_2, the previously calculated fCO_2-T values (**Equation 2**) are added back to the reconstructed fCO_2-Residual and ΔfCO_2-Residual values, and for the latter, CO_2 is also added back (**Equation 3**). All results shown are reconstruction in terms of fCO_2. The full-field reconstructed fCO_2 is used to calculate air-sea CO_2 fluxes (**Section 2.5**)

2.2 Observation-based Reconstructions

We present three observation-based reconstructions: Residual^{ORG}, Residual^{OPT} and ΔResidual^{OPT}. The sole difference between Residual^{ORG} and Residual^{OPT} is the hyperparameters used during algorithmic training (**Table 1**). The main difference between Residual^{ORG}/Residual^{OPT} and ΔResidual^{OPT} is the choice of target variable for the algorithm (fCO_2-Residual vs. ΔfCO_2-Residual; **Equation 2** vs. **Equation 2 & 3**).

Algorithm hyperparameters for Residual^{ORG} are from Bennington et al. (2022a) and include a maximum depth level of 9, a learning rate of 0.3 and 1,000 decision trees (**Table 1**). These hyperparameters were identified based on a nested 3-fold cross-validation grid search with mean squared error as the error metric. Bias-optimized algorithm hyperparameters for Residual^{OPT} are from Heimdal et al. (2025), and include a maximum depth level of 6, a learning rate of 0.3 and 4,000 decision trees (**Table 1**), and are based on algorithm optimization using the CMIP6-testbed (see also **Section 2.3**). Algorithm hyperparameters for ΔResidual are based on algorithm optimization using the delta approach applied to the CMIP6-testbed, and include a maximum depth level of 6, a learning rate of 0.05 and 2,000 decision trees (see **Table 2**; CanESM-CanOE; rightmost value). These hyperparameters were identified as those leading to the smallest 'ESM mean' reconstruction biases throughout the whole analysis period, and represent the hyperparameter combination selected by the ESM CanESM5-CanOE (for more details, see section **S1** and **Fig. S1** in the **Supplementary Material**).

Data used for all three approaches include 1982-2023 monthly 1°x1° gridded fCO_2 observations in SOCATv2024 (Bakker et al., 2024) and predictor variables from various reanalysis products based on observations (see Bennington et al. 2022a). NOAA's globally averaged marine surface monthly mean xCO_2 data (Lan et al. 2025) and ERA5 sea level pressure (Hersbach et al., 2020) is used for the ΔfCO_2 calculation (**Equation 3**). The reconstruction process is repeated five times for each of the three approaches. This is done to reduce the impact stochastic variability in model initialization and training. The results presented in the following sections represent a mean of this ensemble of five reconstructions.

For all three approaches, we use monthly mean values of xCO_2 that include the global average seasonal cycle (i.e., "average" column in the NOAA file). This is a slight deviation from the smoothed xCO_2 used in Bennington et al. (2022a). This is done in order to maintain consistency between the CMIP6-testbed and observation-based approaches. The impact of this change is minimal (global 1982-2023 mean flux difference is 0.01 PgC/yr).

Observation-based approach	Learning rate	Max. depth	Decision trees
$Residual^{ORG}$	0.3	9	1000
$Residual^{OPT}$	0.3	6	4000
$\Delta Residual^{OPT}$	0.05	6	2000

Table 1. *Hyperparameters for the three observation-based approaches. Hyperparameters for* $Residual^{ORG}$ *are from Bennington et al. (2022a) and for* $Residual^{OPT}$ *from Heimdal et al. (2025). Hyperparameters for* $\Delta Residual^{OPT}$ *are from this study.*

2.3 CMIP6-testbed Reconstructions

We use the CMIP6-testbed (Heimdal et al., 2025) to evaluate the fidelity of the fCO_2-Residual method (Bennington et al., 2022a) based on the three approaches ($Residual^{ORG}$, $Residual^{OPT}$ and $\Delta Residual^{OPT}$). A brief description of the CMIP6-testbed is provided below, but for further details see Heimdal et al. (2025). The CMIP6-testbed includes a total of 44 members from nine independent CMIP6 ESMs, with output covering 1982-2023. For each of the 44 ensemble members, fCO_2 and associated predictor variables from the models are sub-sampled monthly at a 1°x1° resolution, at times and locations equivalent to available data in SOCATv2024. In other words, we apply a sampling mask representing SOCAT observations in the CMIP6-testbed to select the algorithmic training set; the sampling mask is a boolean array where the value of 1 represents one monthly 1°x1° sampling location. The predictors include those described in **Section 2.1** (e.g., SST, MLD), but all variables are from the CMIP6-testbed, also including sea level pressure (i.e., not real world observations). For xCO_2, historical data is used from 1982-2014, and RCP4.5 scenario from 2015-2023. The reconstruction process is repeated individually for each of

the 45 members in the testbed, resulting in a total of 45 reconstructions for each of the three approaches.

Algorithm hyperparameters for the Residual^{ORG} and Residual^{OPT} approaches are from Heimdal et al. (2025). We provide a brief description of the hyperparameter selection process, but for further details see Heimdal et al. (2025) and section **S1** in the **supplementary material**. The hyperparameters used for Residual^{ORG} were identified based on a nested 3-fold cross-validation grid search with mean squared error as the error metric (**Table 2**; leftmost values). This method yields one set of hyperparameters per ESM in the CMIP6-testbed, which is applied to all members of each respective ESM. For Residual^{OPT}, the same set of hyperparameters is applied to all members of the testbed (**Table 2**; middle values). These 'optimized' hyperparameters were identified as those leading to the smallest reconstruction biases in the CMIP6-testbed throughout the whole analysis period (Heimdal et al., 2025). For ΔResidual^{OPT}, hyperparameters were identified based on a nested 3-fold cross-validation grid search with bias as the hyperparameter error metric. This method provides one set of hyperparameters per ESM in the CMIP6-testbed, which is applied to all members of each respective ESM (**Table 2**; rightmost values).

Note that the CMIP6-testbed CO_2 output is in partial pressure (pCO_2) as opposed to fugacity (fCO_2) which is what SOCAT provides. These two parameters are comparable, with differences being about 1.2 μatm lower for fCO_2 compared to pCO_2 (Wanninkhof et al 2022); for simplicity, we refer to fCO_2 throughout the paper.

ESM name	**Learning rate**	**Max. depth**	**Decision trees**
UKESM1-0-LL	0.05/0.3/0.1	10/6/6	4,000/4,000/4,000
ACCESS-ESM1-5	0.05/0.3/0.3	10/6/6	4,000/4,000/4,000
CMCC-ESM2	0.05/0.3/0.1	10/6/6	4,000/4,000/4,000
CESM2-WACCM	0.05/0.3/0.1	10/6/7	4,000/4,000/4,000
CESM2	0.05/0.3/0.1	10/6/7	4,000/4,000/500
CanESM5-CanOE	0.1/0.3/0.05	7/6/6	4,000/4,000/2,000
CanESM5	0.10.3/0.05	7/6/7	4,000/4,000/500

MPI-ESM1-2-LR	0.05/0.3/0.05	10/6/6	4,000/4,000/500
GFDL-ESM4	0.05/0.3/0.05	10/6/10	4,000/4,000/2,000

Table 2. *Hyperparameters for the different Earth System Models in the CMIP6-testbed for the three approaches. Left value: Residual^{ORG}. Middle value: Residual^{OPT}. Right value: ΔResidual^{OPT}. Hyperparameters for Residual^{ORG} and Residual^{OPT} are from Heimdal et al. (2025). Hyperparameters for ΔResidual^{OPT}are from this study.*

2.4 Reconstruction error metrics

2.4.1 Observation-based reconstructions

For the observation-based reconstructions, error statistics are calculated by comparing the test set (20 % of the SOCATv2024 dataset) to the reconstructed fCO_2. The test data is separated from the training data by month following Bennington et al. (2022a). Four months are used for training (e.g., January through April), and the next month (e.g., May) is used for testing. This is repeated throughout the full data set (1982-2023). The starting month steps ahead by one for each of the five runs completed. This approach is chosen so that all months and years are represented in the training set. Test error statistics are calculated for each individual reconstruction, i.e., there is a set of five calculations for each of the three approaches. The test error statistics presented in the following sections represent a mean of the five calculations.

2.4.2 CMIP6-testbed reconstructions

For the CMIP6-testbed, reconstruction bias is calculated by comparing the testbed truth to the full fCO_2 reconstruction, but excluding data used for training. Reconstruction bias is a measure of whether the reconstruction overestimates (positive bias) or underestimates (negative bias) fCO_2, and is calculated as:

$$bias = \overline{reconstruction} - \overline{testbed\ truth}$$

The overbars indicate a mean across all 1°x1° grid cells for a specific area (e.g., globally) and all months over a specific period (e.g., 1982-1987). Reconstruction bias is first calculated for each

individual member of the testbed. For ESMs with more than one member, an 'ESM mean' is calculated, which represents an average of bias for all individual members belonging to each ESM. The 'testbed mean' represents a mean of the nine ESM means.

2. 5 Air-sea CO_2 flux calculations

Air-sea CO_2 fluxes are calculated for the observation-based reconstructions using the quadratic bulk formulation (Garbe et al., 2014, Wanninkhof, 1992; Ho et al., 2006):

Equation 4: $\text{Flux} = k_w \cdot \text{sol} \cdot (fCO_2^{ocn} - fCO_2^{atm}) \cdot (1 - \text{ice})$

where k_w is the gas transfer velocity, sol is the solubility of CO_2 in seawater (in units of mol m^{-3} μatm^{-1}), fCO_2^{ocn} is the fugacity of surface ocean carbon (in µatm), and fCO_2^{atm} (in µatm) is the fugacity of atmospheric CO_2 in the marine boundary layer. fCO_2^{ocn} represents reconstructed fCO_2 values. fCO_2^{atm} is the dry air mixing ratio of atmospheric CO_2 (xCO_2) from the NOAA surface marine boundary layer CO_2 product (Dlugokencky et al., 2019) multiplied by ERA5 sea level pressure (Hersbach et al., 2020) at monthly resolution and applying the water vapor correction and conversion to fCO_2 according to Dickson et al. (2007). To account for the seasonal ice cover in high latitudes, the fluxes are weighted by 1 minus the ice fraction (ice), i.e., the open ocean fraction of a grid cell. Inputs to the flux calculation include EN4.2.2 salinity (Good et al., 2020), SST and sea level pressure from ERA5 (Bell et al. 2021, Hersbach et al., 2023), ice fraction from Met Office Hadley Center HadISST product (Rayner et al., 2003). Surface winds and associated wind scaling factors are from the European Centre for Medium-Range Weather Forecasts (ECMWF ERA5; Hersbach et al., 2020, 2023). Further details about flux calculation methods can be found in Fay et al. (2021). Here, the sign convention used for ocean carbon fluxes is positive fluxes to the atmosphere and negative fluxes to the ocean.

3. Results

3.1 Observation-based Reconstructions

3.1.1 Reconstructed fCO_2

The reconstructions for the three approaches yield similar results for the majority of the studied time period, with differences in annual global mean fCO_2 of generally less than 0.5 µatm over 1988-2022 (**Fig. 1a**). Residual^{OPT} and ΔResidual^{OPT} lead to slightly lower annual mean fCO_2 values in the early 1980s compared to Residual^{ORG}, with a maximum annual global mean difference in 1982 of 3.2 and 4.6 µatm respectively (**Fig. 1a**). The largest regional differences between Residual^{ORG} and the optimized approaches are found in the southeast Pacific Ocean and at high latitudes during the 1980s, and at the high latitudes and southern hemisphere eastern boundary upwelling regions in the 2020s (**Fig. S2**).

3.1.2 Air-sea CO_2 flux

Global mean annual air-sea CO_2 fluxes for the three approaches show overall agreement from 1990 until the last few years of the analysis period (**Fig. 1b**). Compared to Residual^{ORG}, Residual^{OPT} and ΔResidual^{OPT} lead to a stronger ocean carbon sink in the 1980s, and lower carbon uptake in the 2020s. The global mean difference from Residual^{ORG} over the first (1982-1987) and last (2018-2023) six years is 0.4/-0.1 PgC/yr for Residual^{OPT} and 0.6/-0.1 PgC/yr for ΔResidual^{OPT}, respectively. The flux differences shown in the 1980s (i.e., compared to Residual^{ORG}) are most significant in the northern hemisphere (> 30°N; **Fig. S3**), while in the 2020s, the Southern Ocean shows the largest discrepancies (< 30°S; **Fig. S3**).

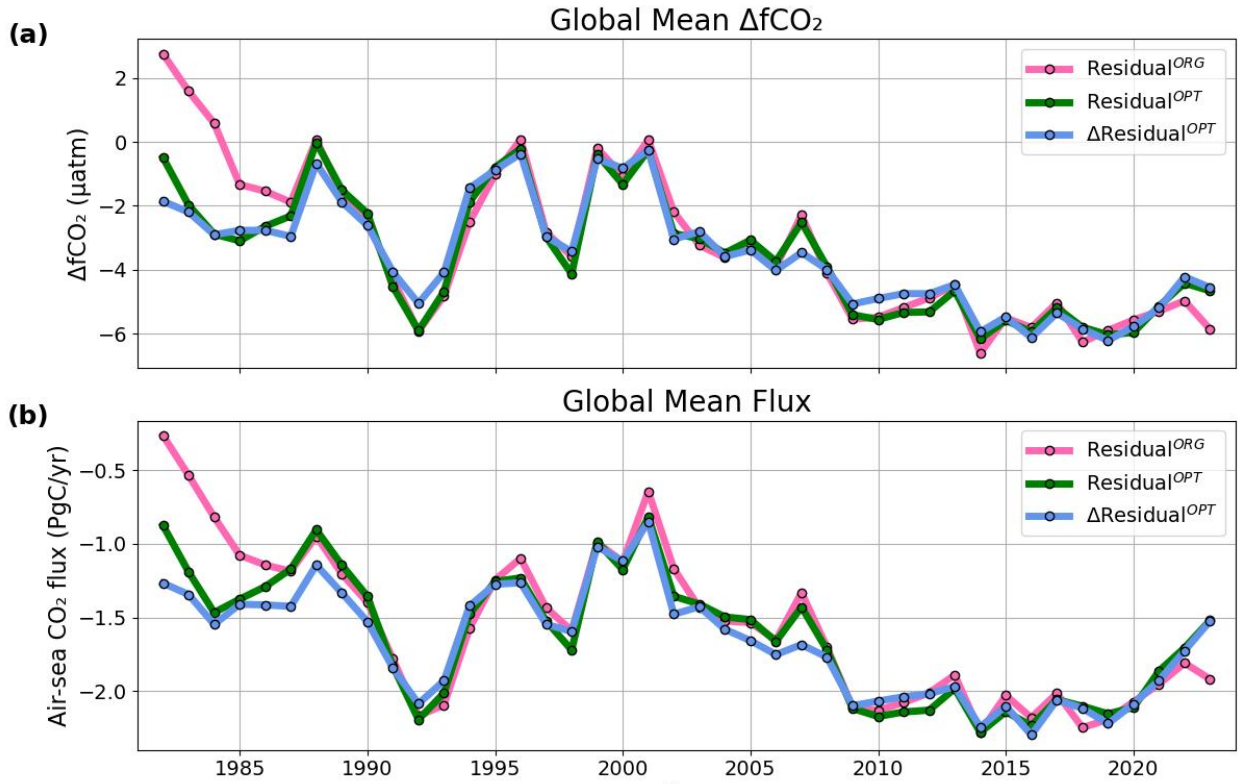

Figure 1: *Annual global, area-weighted, mean ΔfCO_2 (**a**) and air-sea CO_2 flux (**b**) for the Residual-approach (original = pink; optimized = green) versus $\Delta Residual^{OPT}$ (blue). For regional breakdowns of ΔfCO_2 values and air-sea CO_2 fluxes see **Figures S2** and **S3**.*

3.2 Error Metrics

Here we present global mean error metrics for the three approaches, focused on the time periods with the largest discrepancies between the approaches shown by both the observation-based and CMIP6-testbed reconstructions: 1982-1987 and 2018-2023 (**Figs. 1**, **2a**). For the observation-based reconstructions, we compare the predicted fCO_2 to the test set which is a portion of data, unique in each of the five runs, that is withheld from the training (**Section 2.4.1**). We examine the correlation, bias, root mean squared error (RMSE), mean absolute error (Mean AE), and median absolute error (Median AE). For the CMIP6-testbed reconstructions, we compare the predicted fCO_2 to the full testbed truth (**Section 2.4.2**), and present bias as the error metric. Unless otherwise specified, testbed reconstruction bias values presented throughout the paper represent the 'testbed mean', i.e., mean of the full 44-member testbed.

3.2.1 Observation-based test statistics

Overall, the test error metrics suggest similar skill for $Residual^{ORG}$ and $Residual^{OPT}$, with most metrics nearly identical between the two approaches (**Table 3**). The largest difference between these two approaches is in the biases. On the other hand, $\Delta Residual^{OPT}$ shows lower RMSE, mean AE, median AE, absolute bias, and higher correlation for both time periods considered (**Table 3**). The improvement in reconstruction skill shown by $\Delta Residual^{OPT}$ is most significant for 1982-1987, with reductions in error of around 13% for Mean AE, Median AE and RMSE (equivalent to 1.2-2.2 µatm reduction), and 68% for absolute bias (1.5 µatm reduction). All approaches show positive biases over 1982-1987, i.e., fCO_2 is overestimated as compared to the withheld test set. For 2018-2023, $Residual^{ORG}$ shows a negative mean bias of -0.1 µatm, suggesting that this approach underestimates fCO_2, while $Residual^{OPT}$ and $\Delta Residual^{OPT}$ lead to mean biases near zero (**Table 3**). Combined, the observation-based test error metrics suggest that $\Delta Residual^{OPT}$ outperforms both $Residual^{ORG}$ and $Residual^{OPT}$.

Global mean test error metrics for fCO_2 1982-1987 *2018-2023*	$Residual^{ORG}$	$Residual^{OPT}$	$\Delta Residual^{OPT}$
RMSE (µatm)	17.4 *21.1*	17.5 *21.0*	**15.2** ***19.4***
Mean AE (µatm)	12.7 *13.6*	12.8 *13.5*	**11.0** ***12.4***
Median AE (µatm)	9.3 *8.5*	9.6 *8.5*	**8.1** *7.7*
Corr	0.81 *0.89*	0.82 *0.89*	**0.86** ***0.90***
Mean Bias (max./min.) (µatm)	2.2 (0.08/4.0) *-0.1 (-0.7/0.6)*	1.2 (0.3/2.4) ***-0.01*** *(-1.1/0.8)*	**0.6** (-0.4/1.4) *0.04 (-0.5/0.3)*
Absolute bias (µatm)	2.2 *0.4*	1.2 *0.5*	**0.7** ***0.3***

Table 3. *Global mean test error metrics for fCO_2 (top value: 1982-1987; bottom value, in italics: 2018-2023) for the observation-based reconstructions, comparing the three approaches. The error metrics represent a mean of the five individual reconstructions for each approach. Bold values represent the "best" value (i.e., lowest error) for the individual metrics. RMSE = root mean squared error. AE = average error.*

3.2.2 CMIP6–testbed reconstruction bias

As previously shown by Heimdal et al. (2025), $Residual^{ORG}$ leads to an overestimation of fCO_2 (positive bias) in the 1980s, and increasingly negative biases (underestimation of fCO_2) from 2018 and onwards (**Fig. 2a**, pink line). When applying the 'optimized' hyperparameters ($Residual^{OPT}$), the negative biases over 2018-2023 disappear, and the overestimation of fCO_2 in the 1980s is reduced (**Fig. 2a**; pink vs. green lines). However, annual global mean biases are still >1 µatm in the 1980s for $Residual^{OPT}$ (**Table S2**). Here, we find that $\Delta Residual^{OPT}$ is able to further reduce these positive biases (**Fig. 2a**, blue line); the global mean 1982-1987 reconstruction bias for $\Delta Residual^{OPT}$ is only 0.4 µatm, compared to 2 µatm for $Residual^{OPT}$ (**Fig. 2b)**. While there is strong agreement in the annual global mean bias from 1988 and onwards between these two runs (**Fig. 2a**, blue vs. green lines), $\Delta Residual^{OPT}$ shows a slightly smaller spread in bias over 2018-2023 (**Fig. 2c**), the period in which $Residual^{ORG}$ significantly underestimates fCO_2 (**Fig. 2a, c**). Although annual mean biases are near zero in 2018-2023 for both $\Delta Residual^{OPT}$ and $Residual^{OPT}$, small (± 2 µatm) positive and negative biases cancel each other, and larger biases (> 2 µatm) can be found in regions of the Southern Ocean, Indian Ocean, and along coastlines (**Fig. S4)**.

The positive biases shown by $Residual^{ORG}$ in the 1980s occur globally (**Fig. 3**, first column). For both $Residual^{OPT}$ and $\Delta Residual^{OPT}$, there is a reduction in bias across the globe (**Fig. 3**, middle column), however, the biggest improvements (> 2 µatm) for $Residual^{OPT}$ are restricted to the Southern Ocean and North Atlantic (**Fig. 3**, third column, top row), while $\Delta Residual^{OPT}$ shows improvements > 2 µatm throughout the entire Southern Hemisphere and the Atlantic Ocean as well as in the North Pacific (**Fig. 3**, third column, bottom row).

To sum up, the CMIP6-testbed analysis shows that it is possible to reduce the large biases shown for $Residual^{ORG}$ by changing hyperparameters (i.e, $Residual^{OPT}$), particularly for the time period of 2018-2023. However, changing the target variable through the $\Delta Residual^{OPT}$ approach

shows the highest reconstruction skill for the entire analysis period, by significantly reducing biases also in the 1980s. This is also reflected by individual ESMs in the CMIP6-testbed (**Fig. S5**).

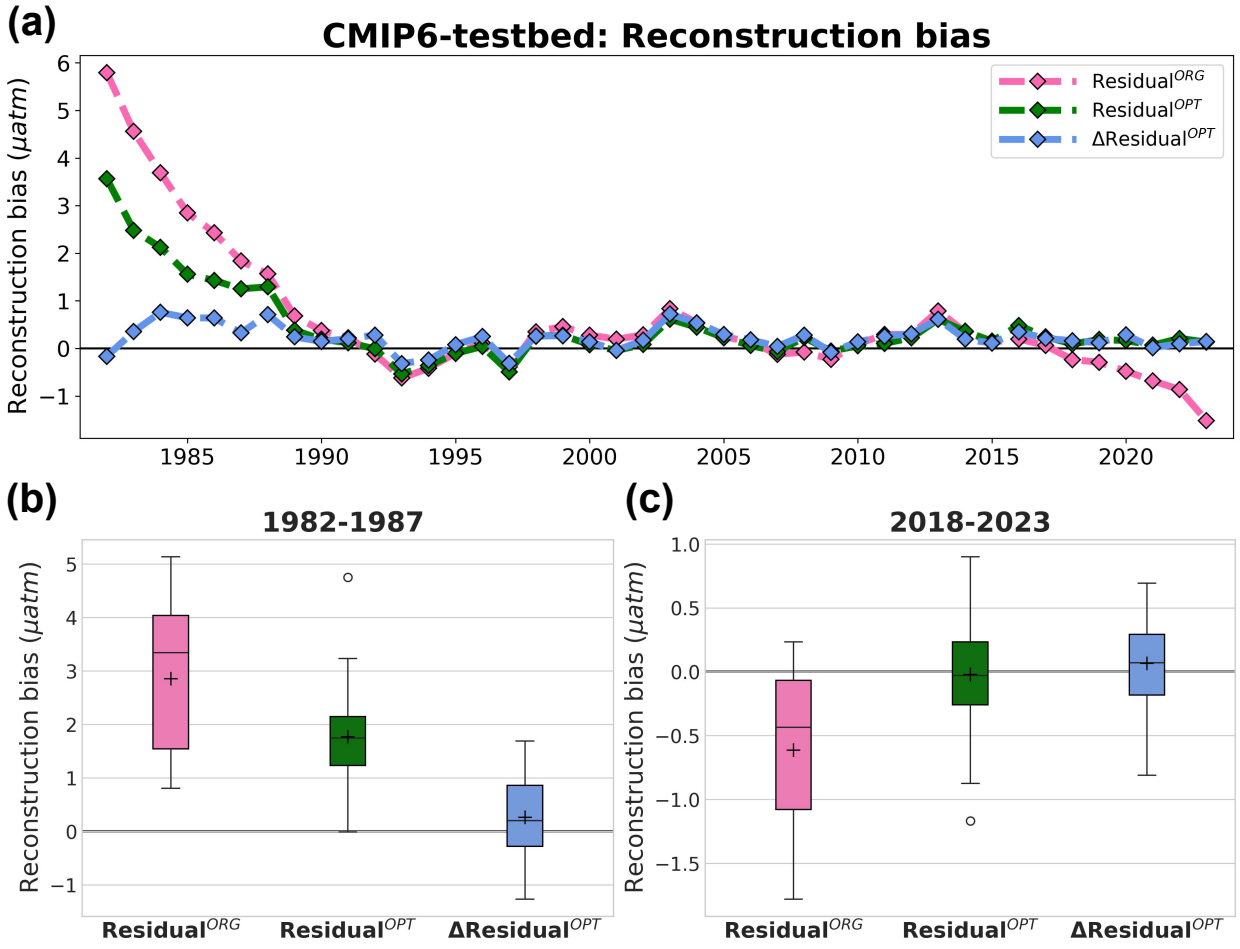

Figure 2: *Annual global mean reconstruction bias timeseries (testbed mean;* ***a****) and testbed spread in global mean reconstruction bias over 1982-1987 (****b****) and 2018-2023 (****c****) for the Residual-approach (original = pink; optimized = green) versus ΔResidual^{OPT} (blue). Large boxes = interquartile range (IQR). Horizontal bars inside boxes = median. Horizontal bars outside boxes = minimum and maximum value. Crosses = mean. Open circles = outliers.*

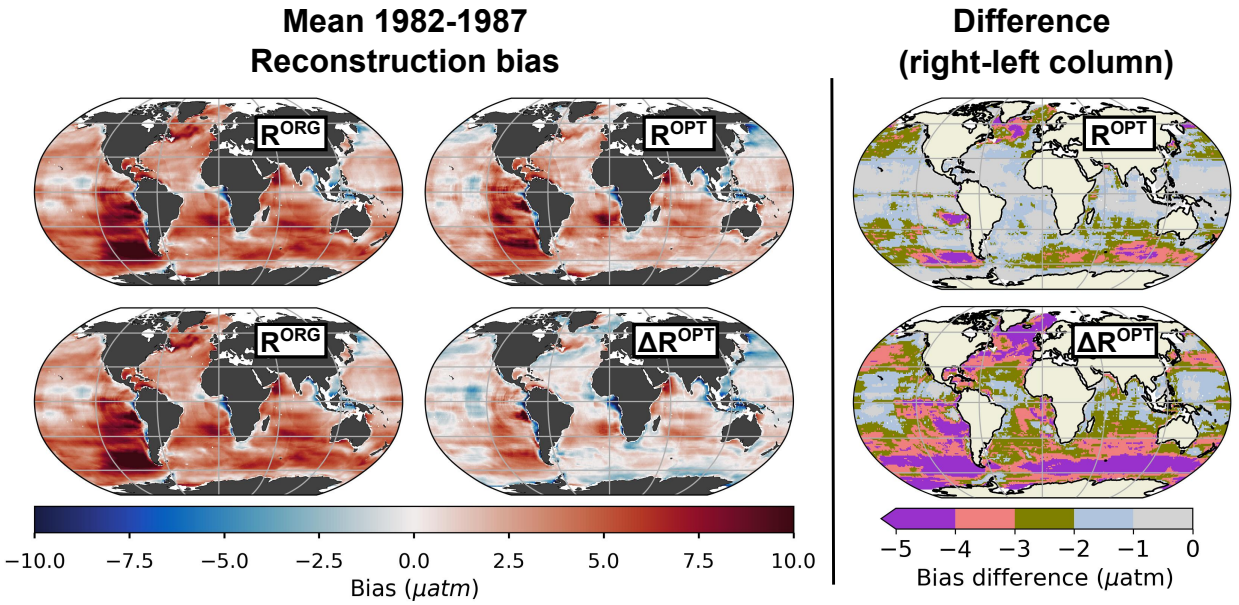

Figure 3: *Spatial mean 1982-1987 reconstruction bias (testbed mean) for Residual^{ORG} (first column, repeated for both rows), Residual^{OPT} (second column, top) and ΔResidual^{OPT} (second column, bottom). Maps in the third column show the difference between the second and first column. Negative values indicate a reduction in bias compared to Residual^{ORG}.*

4. Discussion

4.1 Comparison of the three approaches

We use a suite of metrics to assess the fidelity of the three approaches. Observation-based error metrics are based on the withheld test set which represent only 20% of the SOCATv2024 dataset; however, SOCAT covers only about 2% of the global ocean over the period of 1982-2023. Thus, this test set is admittedly quite small. SOCAT observations are particularly sparse in the 1980s, and have been declining since 2017; therefore, any assessment of reconstruction skill for those years that show the largest errors and discrepancies between approaches (1980s and 2020s) is impacted by the limited data. Spatially, the data sparsity also presents a hurdle as there are large data gaps in the Southern Ocean and much of the Southern Hemisphere. To address this limitation of available data, the additional analysis using the CMIP6-testbed provides a more robust uncertainty analysis, and helps to strengthen our findings despite the limited available data in SOCAT. However, the CMIP6-testbed are simulations for surface fCO_2, not the real world. The benefit of the testbed is that we can compare the full reconstruction to a testbed truth, and we can assess the fidelity of our reconstruction approaches both temporally and spatially. We do this with

multiple ESMs and ensemble members with the goal of spanning across uncertainty due to model structure and internal variability.

Both the observation-based and CMIP6-testbed analyses show positive biases for $Residual^{ORG}$ in the 1980s, and negative biases during the 2020s (**Table 3**, **Fig. 2a**). This suggests that, in the original reconstruction method, the global ocean sink was underestimated in the 1980s, and overestimated in the 2020s. Compared to $Residual^{ORG}$, the global ocean sink over 1982-1987 is increased by 0.4 PgC/yr for $Residual^{OPT}$ and by 0.6 PgC/yr for $\Delta Residual^{OPT}$. Both approaches show a reduction of 0.1 PgC/yr over 2018-2023 (**Fig. 1b**). Both evaluation methods (observation-based and CMIP6-testbed) show smaller reconstruction biases for $Residual^{OPT}$ and $\Delta Residual^{OPT}$ compared to $Residual^{ORG}$ for all time periods considered (**Table 3**, **Figs. 2**, **3**), suggesting that the changes in the reconstructed global ocean sink (i.e., strengthening in the 1980s, and weakening in the 2020s) lead to a more accurate sink estimate.

For the 1980s, both the observation-based and CMIP6-testbed analyses show that $\Delta Residual^{OPT}$ outperforms $Residual^{OPT}$ (**Table 3**, **Figs. 2a,b, 3**). For the CMIP6-testbed, this is the case for both the 'testbed mean' (**Fig. 2a**) and 'ESM means' (**Fig. S5**), and the reduction in bias is not restricted to specific regions, but occurs throughout most of the global ocean (**Fig. 3**). While all observation-based test error metrics show higher skill for $\Delta Residual^{OPT}$ over 2018-2023 (**Table 3**), the CMIP6-testbed analysis shows almost identical reconstruction biases from 1990 and onwards (**Fig. 2a**), although there is a slightly smaller spread for $\Delta Residual^{OPT}$ in 2018-2023 (**Fig. 2c**).

We find generally small differences between $Residual^{OPT}$ and $\Delta Residual^{OPT}$ in terms of reconstructed fCO_2 (**Fig. 1a**) and the estimated air-sea CO_2 flux (**Fig. 1b**); the sink estimates are virtually the same after 1990. In the CMIP6-testbed, reconstruction biases for both these approaches are close to the testbed truth, with annual mean reconstruction biases generally between ± 0.3 μatm (**Fig. 2a**). This suggests that, for the majority of the analysis period, with the appropriate algorithm optimization (as is done in $Residual^{OPT}$), it is possible to improve the air-sea CO_2 flux estimates without removing the long-term trend of fCO_2 from the algorithm target (as is done in $\Delta Residual^{OPT}$). However, taking the full analysis period into account, from 1982-2023, $\Delta Residual^{OPT}$ shows the highest reconstruction skill. This suggests that, even though the flux differences are minor, switching the target variable from fCO_2 to ΔfCO_2 yields a more accurate reconstruction when applying the LDEO-Residual method.

Our results are in agreement with two recent studies that also show reduced reconstruction error when switching the algorithm target variable from fCO_2 to ΔfCO_2 (Gregor et al., 2024; Wanninkhof et al., 2025). Comparable to our results, Wanninkhof et al. (2025) show that the most significant impacts occur during the early years of their reconstruction (1998-2003) and that removing the long-term trend of fCO_2 before reconstruction leads to increased carbon uptake, suggesting that previous sink estimates were underestimated for this time period. We note that these two previous studies applied the delta method to data products that use different algorithms than XGBoost as used here; OceanSODA-ETHZv2 uses a neural network (Gregor et al., 2024) and AOML-ET uses random forest (Wanninkhof et al., 2025). This therefore suggests that removing the long-term trend of fCO_2 from the algorithm target variable leads to reduced reconstruction error and more accurate surface ocean fCO_2 reconstructions for a range of data products and algorithms.

4.2 Comparison to Global Carbon Budget (GCB) ocean sink estimates

We compare the observation-based air-sea CO_2 fluxes calculated for the three approaches to those from GOBMs and data products alongside GCB merged model/product mean with estimated +/- 0.4 PgC/yr uncertainty bounds (**Fig. 4**). These values are all presented in the 2024 GCB paper (Friedlingstein et al., 2025). All data product fluxes in **Figure 4** are adjusted assuming a riverine carbon flux of 0.65 Gt C/yr following Friedlingstein et al. (2025) in order to compare with GOBM fluxes.

For the period of 1982-1987, $Residual^{ORG}$ shows a smaller sink than the ensemble of data products and models, falling outside of the GCB mean uncertainty as well (**Fig. 4**). Combined with the strong positive biases shown for this approach by both the observation-based reconstruction and the CMIP6-testbed, we conclude that $Residual^{ORG}$ likely underestimates the global ocean sink for this time period. $\Delta Residual^{OPT}$, which shows the strongest global mean sink out of our three approaches for this early time period, falls close to the ensemble mean of the data products, but shows a slightly weaker sink. The small positive biases shown for this approach in the 1980s, suggesting that the $\Delta Residual^{OPT}$ likely slightly underestimates the sink, points towards that the data product ensemble mean might be quite close to the truth in the 1980s.

Over 1990-2020, all three LDEO- Residual approaches behave similarly, and generally fall within the uncertainty bounds of the GCB mean (**Fig.4**). In the early 1990s and 2000s, the three LDEO-Residual approaches plot on the higher (strongest sink) and lower (weakest sink) end of the GCB mean ocean sink estimate, with some approaches falling outside of the uncertainty spread. Interestingly, the CMIP6-testbed shows small, but distinct negative (positive) biases for the same time periods (-0.6 µatm in 1993 and 0.8 µatm in 2003; **Table S2**, **Fig. 2a**), which would suggest an overestimation (underestimation) of the carbon sink. Following the "peak" in the early 2000s, the three LDEO-Residual approaches fall close to the GOBM ensemble mean, and show a weaker sink than the majority of the data products, especially in the last decade. By using the CMIP6-testbed, we have shown that our preferred approach ($\Delta Residual^{OPT}$) is able to reconstruct the decadal variability of the global mean surface ocean fCO_2 reasonably well, with annual mean biases of generally ± 0.3 µatm (**Table S2**, **Fig. 2**). The comparison in **Figure 4** thus suggests that the current data products in the GCB may overestimate the global ocean sink from 2010 and onwards. We show that careful optimization of hyperparameters for all machine learning methods can impact reconstruction flux results considerably and we encourage all data product creators to optimize regularly.

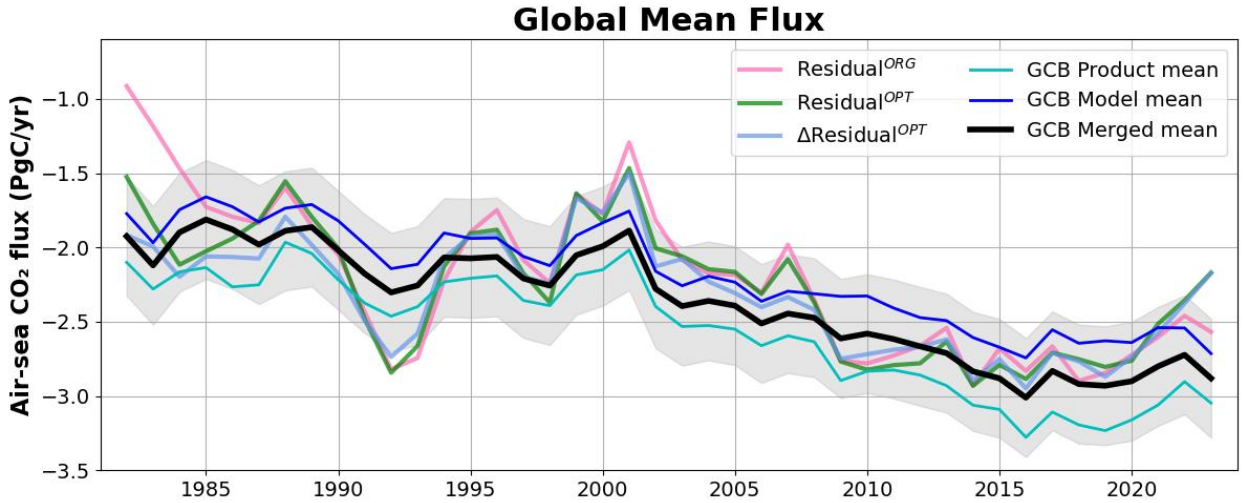

Figure 4: *Annual global mean air-sea CO_2 flux for the three approaches (Same as* ***Figure 1b****, but adjusted for riverine inputs) behind Global Carbon Budget (GCB) data products ensemble mean (cyan), GOBM ensemble mean (blue), and merged model/product mean (black) with estimated +/- 0.4 PgC/yr uncertainty bounds (gray shading). GCB values from Friedlingstein et al. 2025. Residual-approach colors: Residual^{ORG} = pink; Residual^{OPT} = green, ΔResidual^{OPT} = light blue.*

5. Conclusions

To synthesize, $\Delta Residual^{OPT}$ leads to the highest reconstruction skill throughout the entire analysis period (1982-2023), shown by both observation-based test error metrics and the CMIP6-testbed; largest improvements in reconstruction skill are seen in the 1980s. This suggests that removing the long-term trend of fCO_2, by using ΔfCO_2-Residual as the algorithm target variable, leads to a more accurate estimate of global ocean carbon uptake. Compared to $Residual^{ORG}$ (Bennington et al., 2022a), the global ocean carbon sink is increased by 0.6 Pg C/yr over 1982-1987 and decreased by 0.1 Pg C/yr over 2018-2023. We also show that, from 1990 and onwards, by optimizing the algorithm hyperparameters, it is possible to improve reconstruction skill and air-sea CO_2 flux estimates without removing the long-term trend of fCO_2 from the algorithm target variable ($Residual^{OPT}$). We conclude that, for the LDEO fCO_2-Residual method, the impacts of algorithmic design choices, i.e., the choice of target variable or hyperparameters, on reconstruction skill and estimated air-sea CO_2 fluxes are significant, and the improved reconstruction fidelity ($\Delta Residual^{OPT}$) will be carried out in future releases.

Code availability

Data analysis scripts and supporting files for the observation-based pCO_2-Residual method are publicly available at https://github.com/OceanCarbon-LDEO-Columbia/. Code for running CMIP6-testbed experiments is publicly available at https://zenodo.org/records/16645455 (Shaum and Heimdal, 2025). Detailed information on how to access and/or download the CMIP6-testbed is publicly available at https://zenodo.org/records/16654165 (Heimdal, 2025). Code for producing all figures presented in this manuscript will be publicly available upon publication.

Data availability

This publication uses the Pangeo-ESGF CMIP6 Zarr Data 2 (Busecke and Stern, 2024).

Competing interests

The authors declare that they have no conflict of interest.

Acknowledgements

We acknowledge funding from NOAA (Award #NA20OAR4310340), the European Space Agency via subaward from University of Exeter and NSF through the OCE Award #2333608 and the LEAP STC Award #2019625. We acknowledge the computing and storage resources provided by LEAP. We acknowledge support from Schmidt Sciences, LLC, and thank the $COCO_2$ team for their collective efforts in data collection and machine learning development. VA acknowledges support from a PIVOT fellowship grant (Award #981849) and a PIVOT Research award (#12871) from the Simons Foundation. The authors acknowledge the World Climate Research Programme, which, through its Working Group on Coupled Modelling, coordinated and promoted CMIP6. The authors thank the climate modeling groups for producing and making available their model output, the Earth System Grid Federation (ESGF) for archiving the data and providing access, and the multiple funding agencies who support CMIP6 and ESGF. The Surface Ocean CO_2 Atlas (SOCAT) is an international effort, endorsed by the International Ocean Carbon Coordination Project (IOCCP), the Surface Ocean Lower Atmosphere Study (SOLAS) and the Integrated Marine Biosphere Research (IMBeR) program, to deliver a uniformly quality-controlled surface ocean CO_2 database. The many researchers and funding agencies responsible for the collection of data and quality control are thanked for their contributions to SOCAT.

References

Bakker, D. C. E., Pfeil, B., Landa, C. S., Metzl, N., O'Brien, K. M., Olsen, A., Smith, K., Cosca, C., Harasawa, S., Jones, S. D., Nakaoka, S., Nojiri, Y., Schuster, U., Steinhoff, T., Sweeney, C., Takahashi, T., Tilbrook, B., Wada, C., Wanninkhof, R., Alin, S. R., Balestrini, C. F., Barbero, L., Bates, N. R., Bianchi, A. A., Bonou, F., Boutin, J., Bozec, Y., Burger, E. F., Cai, W.-J., Castle, R. D., Chen, L., Chierici, M., Currie, K., Evans, W., Featherstone, C., Feely, R. A., Fransson, A., Goyet, C., Greenwood, N., Gregor, L., Hankin, S., Hardman-Mountford, N. J., Harlay, J., Hauck, J., Hoppema, M., Humphreys, M. P., Hunt, C. W., Huss, B., Ibánhez, J. S. P., Johannessen, T., Keeling, R., Kitidis, V., Körtzinger, A., Kozyr, A., Krasakopoulou, E., Kuwata, A., Landschützer, P., Lauvset, S. K., Lefèvre, N., Lo Monaco, C., Manke, A., Mathis, J. T., Merlivat, L., Millero, F. J., Monteiro, P. M. S., Munro, D. R., Murata, A., Newberger, T., Omar, A. M., Ono, T., Paterson, K., Pearce, D., Pierrot, D., Robbins, L. L., Saito, S., Salisbury, J., Schlitzer, R., Schneider, B., Schweitzer, R., Sieger, R., Skjelvan, I., Sullivan, K. F., Sutherland, S. C., Sutton, A. J., Tadokoro,

K., Telszewski, M., Tuma, M., van Heuven, S. M. A. C., Vandemark, D., Ward, B., Watson, A. J., and Xu, S.: A multi-decade record of high-quality fCO_2 data in version 3 of the Surface Ocean CO_2 Atlas (SOCAT), Earth System Science Data, 8, 383–413, https://doi.org/10.5194/essd-8-383-2016, 2016.

Bakker, Dorothee C. E.; Alin, Simone R.; Bates, Nicholas; Becker, Meike; Gkritzalis, Thanos; Jones, Steve D.; Kozyr, Alex; Lauvset, Siv K.; Metzl, Nicolas; Nakaoka, Shin-ichiro; O'Brien, Kevin M.; Olsen, Are; Pierrot, Denis; Steinhoff, Tobias; Sutton, Adrienne J.; Takao, Shintaro; Tilbrook, Bronte; Wada, Chisato; Wanninkhof, Rik; Akl, John; Arbilla, Lisandro A.; Arruda, Ricardo; Azetsu-Scott, Kumiko; Barbero, Leticia; Beatty, Cory M.; Berghoff, Carla F.; Bittig, Henry C.; Burger, Eugene F.; Campbell, Katie; Cardin, Vanessa; Collins, Andrew; Coppola, Laurent; Cronin, Margot; Cross, Jessica N.; Currie, Kim I.; Emerson, Steven R.; Enright, Matt P.; Enyo, Kazutaka; Evans, Wiley; Feely, Richard A.; Flohr, Anita; Gehrung, Martina; Glockzin, Michael; González-Dávila, Melchor; Hamnca, Siyabulela; Hartman, Sue; Howden, Stephan D.; Kam, Kitty; Kamb, Linus; Körtzinger, Arne; Kosugi, Naohiro; Lefèvre, Nathalie; Lo Monaco, Claire; Macovei, Vlad A.; Maenner Jones, Stacy; Manalang, Dana; Martz, Todd R.; Mdokwana, Baxolele; Monacci, Natalie M.; Monteiro, Pedro M. S.; Mordy, Calvin; Morell, Julio M.; Murata, Akihiko; Neill, Craig; Noh, Jae-Hoon; Nojiri, Yukihiro; Ohman, Mark D.; Olivier, Léa; Ono, Tsuneo; Petersen, Wilhelm; Plueddemann, Albert J.; Prytherch, John; Rehder, Gregor; Rutgersson, Anna; Santana-Casiano, J. Magdalena; Schlitzer, Reiner; Send, Uwe; Skjelvan, Ingunn; Sullivan, Kevin F.; T'Jampens, Michiel; Tadokoro, Kazuaki; Telszewski, Maciej; Theetaert, Hannelore; Tsanwani, Mutshutshu; Vandemark, Douglas; van Ooijen, Erik; Veccia, Martín H.; Voynova, Yoana G.; Wang, Hongjie; Weller, Robert A.; Woosley, Ryan J. (2024). Surface Ocean CO2 Atlas Database Version 2024 (SOCATv2024) (NCEI Accession 0293257). NOAA National Centers for Environmental Information. Dataset. https://doi.org/10.25921/9wpn-th28. Accessed June 28, 2024.

Behncke, J., Landschützer, P. & Tanhua, T. A detectable change in the air-sea CO_2 flux estimate from sailboat measurements, *Scientific Reports*, 14, 3345, https://doi.org/10.1038/s41598-024-53159-0 (2024).

Bell, B., Hersbach, H., Simmons, A., Berrisford, P., Dahlgren, P., Horányi, A., Muñoz-Sabater, J., Nicolas, J., Radu, R., Schepers, D. and Soci, C., The ERA5 global reanalysis: Preliminary extension to 1950. Quarterly Journal of the Royal Meteorological Society, 147(741), pp.4186-4227, 2021.

Bennington, V., Galjanic, T., and McKinley, G. A.: Explicit Physical Knowledge in Machine Learning for Ocean Carbon Flux Reconstruction: The pCO_2-Residual Method, Journal of Advances in Modeling Earth Systems, 14(10), https://doi.org/10.1029/2021ms002960, 2022a.

Bennington, V., Gloege, L., and McKinley, G. A.: Variability in the global ocean carbon sink from 1959 to 2020 by correcting models with observations, Geophysical Research Letters, 49(14), https://doi.org/10.1029/2022GL098632, 2022b.

Busecke, J. J. M., and Stern, C. I.: cmip6-leap-feedstock (v0.2.0), Zenodo, https://doi.org/10.5281/zenodo.10621538, 2024.

Chen, T., and Guestrin, C.: Xgboost: A scalable tree boosting system, In: Proceedings of the 22nd ACM SIGKDD international conference on knowledge discovery and data mining (pp. 785-794), https://doi.org/10.1145/2939672.2939785, 2016.

Dickson, A.G., Sabine, C.L., and Christian, J.R. (Eds): Guide to best practices for ocean CO2 measurement. Sidney, British Columbia, North Pacific Marine Science Organization, 191 pp. (PICES Special Publication3; IOCCP Report 8), https://doi.org/10.25607/OBP-1342, 2007.

Dlugokencky, E.J., Thoning, K.W., Lang, P.M., and Tans, P.P.: NOAA greenhouse gas reference from atmospheric carbon dioxide dry air mole fractions from the NOAA ESRL carbon cycle cooperative global air sampling network, 2019 (data available at: https://gml.noaa.gov/ccgg/mbl/data.php, last access: 22 October 2024).

Dong, Y., Bakker, D. C. E., Bell, T. G., Yang, M., Landschützer, P., Hauck, J., Rödenbeck, C., Kitidis, V., Bushinsky, S. M., and Luss, P. S.: Direct observational evidence of strong CO_2 uptake in the Southern Ocean, Science Advances, 10, eadn5781, DOI: 10.1126/sciadv.adn5781, 2024.

Fay, A. R., Gregor, L., Landschützer, P., McKinley, G. A., Gruber, N., Gehlen, M., Iida, Y., Laruelle, G. G., Rödenbeck, C., Roobaert, A., and Zeng, J.: SeaFlux: harmonization of air-sea CO_2 fluxes from surface pCO_2 data products using a standardized approach, Earth System Science Data, 13, 4693-4710, https://doi.org/10.5194/essd-13-4693-2021, 2021.

Fay, A. R., Heimdal, T. H., Acquaviva, V., Shaum, A. P., and McKinley, G. A.: Sensitivity of ocean carbon sink estimates to rare observations, Geophysical Research Letters, 52(19), https://doi.org/10.1029/2025GL117961, 2025.

Ford, D., Blannin, J., Watts, J., Watson, A., Landschützer, P., Jersild, A., and Shutler, J.: A comprehensive analysis of air-sea CO_2 flux uncertainties constructed from surface ocean data products, Global Biogeochem. Cycles, 38, e2024GB008188, https://doi.org/10.1029/2024GB008188, 2024.

Friedlingstein, P., O'Sullivan, M., Jones, M. W., Andrew, R. M., Hauck, J., Landschützer, P., Le Quéré, C., Li, H., Luijkx, I. T., Olsen, A., Peters, G. P., Peters, W., Pongratz, J., Schwingshackl, C., Sitch, S., Canadell, J. G., Ciais, P., Jackson, R. B., Alin, S. R., Arneth, A., Arora, V., Bates, N. R., Becker, M., Bellouin, N., Berghoff, C. F., Bittig, H. C., Bopp, L., Cadule, P., Campbell, K., Chamberlain, M. A., Chandra, N., Chevallier, F., Chini, L. P., Colligan, T., Decayeux, J., Djeutchouang, L. M., Dou, X., Duran Rojas, C., Enyo, K., Evans, W., Fay, A. R., Feely, R. A., Ford, D. J., Foster, A., Gasser, T., Gehlen, M., Gkritzalis, T., Grassi, G., Gregor, L., Gruber, N., Gürses, Ö., Harris, I., Hefner, M., Heinke, J., Hurtt, G. C., Iida, Y., Ilyina, T., Jacobson, A. R., Jain, A. K., Jarníková, T., Jersild, A., Jiang, F., Jin, Z., Kato, E., Keeling, R. F., Klein Goldewijk, K., Knauer, J., Korsbakken, J. I., Lan, X., Lauvset, S. K., Lefèvre, N., Liu, Z., Liu, J., Ma, L., Maksyutov, S., Marland, G., Mayot, N., McGuire, P. C., Metzl, N., Monacci, N. M., Morgan, E. J., Nakaoka, S.-I., Neill, C., Niwa, Y., Nützel, T., Olivier, L., Ono, T., Palmer, P. I., Pierrot, D., Qin, Z., Resplandy, L., Roobaert, A., Rosan, T. M., Rödenbeck, C., Schwinger, J., Smallman, T.

L., Smith, S. M., Sospedra-Alfonso, R., Steinhoff, T., Sun, Q., Sutton, A. J., Séférian, R., Takao, S., Tatebe, H., Tian, H., Tilbrook, B., Torres, O., Tourigny, E., Tsujino, H., Tubiello, F., van der Werf, G., Wanninkhof, R., Wang, X., Yang, D., Yang, X., Yu, Z., Yuan, W., Yue, X., Zaehle, S., Zeng, N., and Zeng, J.: Global Carbon Budget 2024, Earth Syst. Sci. Data, 17, 965–1039, https://doi.org/10.5194/essd-17-965-2025, 2025.

Garbe, C. S., Rutgersson, A., Boutin, J., Leeuw, G. D., Delille, B., Fairall, C. W., Gruber, N., Hare, J., Ho, D. T., Johnson, M. T., Nightingale, P. D., Pettersson, H., Piskozub, J., Sahleé, E., Tsai, W., Ward, B., Woolf, D. K., and Zappa, C. J.: Transfer across the air-sea interface, in: Ocean-Atmosphere Interactions of Gases and Particles, edited by: Liss, P. S. and Johnson, M. T., Springer, Berlin, Heidelberg, 55–112, 2014.

Gloege, L., McKinley, G. A., Landschützer, P., Fay, A. R., Frolicher, T. L., and Fyfe, J. C.: Quantifying Errors in Observationally Based Estimates of Ocean Carbon Sink Variability, Global Biogeochemical Cycles, 35(4), https://doi.org/10.1029/2020gb006788, 2021.

Gloege, L., Yan, M., Zheng, T. and McKinley, G. A.: Improved quantification of ocean carbon uptake by using machine learning to merge global models and pCO_2 data, Journal of Advances in Modeling Earth Systems, 14(2), https://doi.org/10.1029/2021MS002620, 2022.

Good, S. A., Martin, M. J., and Rayner, N. A.: EN4: Quality controlled ocean temperature and salinity profiles and monthly objective analyses with uncertainty estimates, Journal of Geophysical Research: Oceans, 118, 6704–6716, https://doi.org/10.1002/2013JC009067, 2013.

Gregor, L., Shutler, J., and Gruber, N.: High-resolution variability of the ocean sink, Global Biogeochemical Cycles, 38, 8, e2024GB008127, https://doi.org/10.1029/2024GB008127, 2024.

Goodfellow I., Bengio Y., and Courville A.: Deep Learning (MIT Press), 2016 (available at: http://www.deeplearningbook.org)

Hauck, J., Nissen, C., Landschützer, P., Rödenbeck, C., Bushinsky, S., and Olsen, A.: Sparse observations induce large biases in estimates of the global ocean CO2 sink: and ocean model sub-

sampling experiment, Philosophical Transactions Of the Royal Society A, 381:20220063, https://doi.org/10.1098/rsta.2022.0063, 2023.

Heimdal, T.H.: Overview of the CMIP6-testbed (Version v1), Zenodo, https://zenodo.org/records/16654165, 2025.

Heimdal, T. H., McKinley, G. A., Sutton, A. J., Fay, A. R., and Gloege, L.: Assessing improvements in global ocean pCO_2 machine learning reconstructions with Southern Ocean autonomous sampling, Biogeosciences, 21, 2159-2176, https://doi.org/10.5194/bg-21-2159-2024, 2024.

Heimdal, T. H., and McKinley, G. A.: Using observing system simulation experiments to assess impacts of observational uncertainties in surface ocean pCO_2 machine learning reconstructions, Scientific Reports, 14, 19763, https://doi.org/10.1038/s41598-024-70617-x, 2024.

Heimdal, T. H., Shaum A. P., Acquaviva V., Fay, A. R., Samant, D., Busecke, J., and McKinley, G. A.: Targeting bias in algorithm optimization improves reconstructions of surface ocean pCO_2, Machine Learning: Earth, https://doi.org/10.31223/X5H727, 2025.

Hersbach, H., Bell, B., Berrisford, P., Hirahara, S., Horányi, A., Muñoz-Sabater, J., Nicolas, J., Peubey, C., Radu, R., Schepers, D., Simmons, A., Soci, C., Abdalla, S., Abellan, X., Balsamo, G., Bechtold, P., Biavati, G., Bidlot, J., Bonavita, M., De Chiara, G., Dahlgren, P., Dee, D., Diamantakis, M., Dragani, R., Flemming, J., Forbes, R., Fuentes, M., Geer, A., Haimberger, L., Healy, S., Hogan, R.J., Hólm, E., Janisková, M., Keeley, S., Laloyaux, P., Lopez, P., Lupu, C., Radnoti, G., de Rosnay, P., Rozum, I., Vamborg, F., Villaume, S., and Thépaut, J.: The ERA5 global reanalysis, Quarterly Journal of the Royal Meteorological Society, 146, 1999–2049, https://doi.org/10.1002/qj.3803, 2020 (data available at: https://cds.climate.copernicus.eu/cdsapp#!/dataset/reanalysis-era5-single-levels-monthly-means?tab=overview).

Hersbach, H., Bell, B., Berrisford, P., Biavati, G., Horányi, A., Muñoz Sabater, J., Nicolas, J., Peubey, C., Radu, R., Rozum, I., Schepers, D., Simmons, A., Soci, C., Dee, D., Thépaut, J-N.: ERA5 hourly data on single levels from 1940 to present, Copernicus Climate Change Service (C3S) Climate Data Store (CDS), DOI: 10.24381/cds.adbb2d47 (Accessed on 20-07-2023), 2023.

Ho, D. T., Law, C. S., Smith, M. J., Schlosser, P., Harvey, M., and Hill, P.: Measurements of airsea gas exchange at high wind speeds in the Southern Ocean: Implications for global parameterizations, Geophys. Res. Lett., 33, L16611, https://doi.org/10.1029/2006GL026817, 2006.

Iida, Y., Takatani, Y., Kojima, A., and Ishii, M.: Global trends of ocean CO_2 sink and ocean acidification: an observation-based reconstruction of surface ocean inorganic carbon variables, Journal of Oceanography, 77, 323–358, https://doi.org/10.1007/s10872-020-00571-5, 2021.

Landschützer, P., Gruber, N., and Bakker, D. C. E.: Decadal variations and trends of the global ocean carbon sink: decadal air-sea CO_2 flux variability, Global Biogeochem. Cy., 30, 1396–1417, https://doi.org/10.1002/2015GB005359, 2016.

Rayner, N. A., Parker, D. E., Horton, E. B., Folland, C. K., Alexander, L. V., Rowell, D. P., & Kaplan, A.: Global analyses of sea surface temperature, sea ice, and night marine air temperature since the late nineteenth century. Journal of Geophysical Research, 108(D14), 4407. https://doi.org/10.1029/2002JD002670, 2003.

Rödenbeck, C., DeVries, T., Hauck, J., Le Quéré, C., and Keeling, R. F.: Data-based estimates of interannual sea–air CO_2 flux variations 1957–2020 and their relation to environmental drivers, Biogeosciences, 19, 2627–2652, https://doi.org/10.5194/bg-19-2627-2022, 2022.

Shaum, A., and Heimdal, T.H.: Code for ML reconstruction of surface ocean pCO_2 using the CMIP6-testbed (Version v1), Zenodo, https://zenodo.org/records/16645455, 2025.

Takahashi, T., Sutherland, S.C., Sweeney, C., Poisson, A., Metzl, N., Tilbrook, B., Bates, N.,

Wanninkhof, R., Feely, R.A., Sabine, C. and Olafsson, J., Global sea–air CO2 flux based on climatological surface ocean pCO2, and seasonal biological and temperature effects. Deep Sea Research Part II: Topical Studies in Oceanography, 49(9-10), pp.1601-1622, https://doi.org/10.1016/S0967-0645(02)00003-6, 2002.

Wanninkhof, R.: Relationship between wind speed and gas exchange over the ocean, J. Geophys. Res., 97, 7373, https://doi.org/10.1029/92JC00188, 1992

Wanninkhof, R., Pierrot, D., Sullivan, K., Mears, P., & Barbero, L., Comparison of discrete and underway CO2 measurements: Inferences on the temperature dependence of the fugacity of CO_2 in seawater. Marine Chemistry, 247, 104178. https://doi.org/10.1016/j.marchem.2022.104178, 2022.

Wanninkhof, R., Triñanes, J., Pierrot, D., Munro, D.R., Sweeney, C. and Fay, A.R., Trends in sea-air CO2 fluxes and sensitivities to atmospheric forcing using an extremely randomized trees machine learning approach. Global Biogeochemical Cycles, 39(2), https://doi.org/10.1029/2024GB008315, 2025.

Williams, N. L. *et al*. Calculating surface ocean pCO_2 from biogeochemical Argo floats equipped with pH: An uncertainty analysis, Global Biogeochemical Cycles, 31(3), 591-604, https://doi.org/10.1002/2016GB005541, 2017.

Zhong, G., Li, X., Song, J., Wang, F., Qu, B., Wang, Y., Zhang, B., Ma, J., Yuan, H., Duan, L., Wang, Q., Xing, J., and Dai., J.: The Southern Ocean carbon sink has been overestimated in the past three decades, Communications Earth & Environment, 5, 398, https://doi.org/10.1038/s43247-024-01566-6, 2024.